A Superposition Framework for Discrete Dislocation Plasticity

M. P. O'Day

W. A. Curtin
Division of Engineering,
Brown University,
Providence, RI 02912

A superposition technique is introduced that allows for the application of discrete dislocation (DD) plasticity to a wide range of thermomechanical problems with reduced computational effort. Problems involving regions of differing elastic and/or plastic behavior are solved by superposing the solutions to i) DD models only for those regions of the structure where dislocation phenomena are permitted subject to either zero traction or displacement at every point on the boundary and ii) an elastic (EL) (or elastic/cohesive-zone) model of the entire structure subject to all desired loading and boundary conditions. The DD subproblem is solved with standard DD machinery for an elastically homogeneous material. The EL subproblem requires only a standard elastic or elastic/cohesive-zone finite element (FE) calculation. The subproblems are coupled: the negative of the tractions developed at the boundaries of the DD subproblem are applied as body forces in the EL subproblem, while the stress field of the EL subproblem contributes a driving force to the dislocations in the DD subproblem structure. This decomposition and the generic boundary conditions of the DD subproblem permit the DD machinery to be easily applied as a "black-box" constitutive material description in an otherwise elastic FE formulation and to be used in a broader scope of applications due to the overall enhanced computational efficiency. The method is validated against prior results for crack growth along a plastic/rigid bimaterial interface. Preliminary results for crack growth along a metal/ceramic bimaterial interface are presented. [DOI: 10.1115/1.1794167]

1 Introduction

The proliferation of increasingly smaller structures has highlighted the necessity of developing accurate modeling techniques for material deformation at these scales. Currently, micron scale analysis is important for micromachines and microelectronic components, as well as for the fundamental modeling of fracture processes. A wealth of experimental evidence has shown that in metal specimens having characteristic dimensions less than 100 μm, plastic flow exhibits a size effect: smaller is stronger [1,2]. Classical continuum plasticity does not include a length scale, precluding any size effects. Thus the application of classical plastic constitutive laws to micron scale specimens is questionable. The micron-size scale effectively lies in an intermediate regime that is too large for fully atomistic modeling, but small enough that individual dislocation effects are important and cannot be averaged into a classical continuum plasticity constitutive law. Over the last decade several new methods have been developed that can more accurately predict deformation at smaller scales.

Numerous nonlocal plasticity theories have been developed in an attempt to reproduce size effects [3–5]. These theories introduce a length scale that aims to account for the effect of geometrically necessary dislocations. As continuum theories, most nonlocal models can be incorporated into existing finite element (FE) architecture with only slight modifications. However, there remain several drawbacks to nonlocal formulations. Like classical plasticity, these are phenomenological theories that do not account for the fundamental basis of plasticity, i.e., the motion of dislocations. The specification of the various length scales, usually chosen by a fit to experimental data, is also an outstanding issue [6].

An alternative technique is the discrete dislocation (DD) method of Van der Giessen and Needleman [7]. The DD approach solves boundary value problems (bvp) for isotropic elastic bodies containing mobile dislocations, which carry the information about plastic deformation. No assumptions about the material plastic constitutive response are necessary although a set of constitutive rules governing dislocation motion, nucleation, and annihilation are required. The DD method has the benefit of being a true mechanism-based theory of plasticity; plastic flow arises directly from dislocation motion. The DD method has recently been applied to study flow in composites of varying microstructure [8], crack growth in plastic materials [9], fatigue crack growth [10], and size effects in model Al/Si alloys [11]. The DD method has also proven useful in acting as a numerical experiment for comparison with various nonlocal theories [6,12]. One limitation of the method is its significant computational cost, particularly for bodies containing elastic inhomogeneities [7] and/or large numbers of dislocations. For this reason much of the work to date has focused on elastically homogeneous systems, often with some degree of symmetry to further simplify the computation. Consequently, many interesting physical problems that demand noncontinuum treatments have yet to be examined within the powerful DD framework.

Here a new superposition technique is presented that allows for a computationally efficient solution of elastically inhomogeneous DD problems. The problem of interest is solved by superposing the solutions to i) a DD model of only that portion of the structure where dislocation phenomena are permitted subject to special boundary conditions and ii) an elastic (EL) model of the entire structure subject to all desired loading and boundary conditions. The DD subproblem is homogeneous and solved with standard DD machinery, including a contribution to the Peach-Koehler forces on the dislocations coming from the EL subproblem. The EL subproblem is solved with a standard elastic FE calculation including special body forces that emerge from the DD problem. This technique is basically a special application of the Eshelby method [13]. It is similar to the coupled atomistic/continuum method of Shilkrot et al. [14], although here the formulation is purely continuum in nature. The new technique also simplifies the application of the DD method to other problems because it separates out a generic DD subproblem that can be considered as a material constitutive law. Finally, the superposition method is

Contributed by the Applied Mechanics Division of THE AMERICAN SOCIETY OF MECHANICAL ENGINEERS for publication in the ASME JOURNAL OF APPLIED MECHANICS. Manuscript received by the Applied Mechanics Division, February 24, 2003; final revision, October 30, 2003. Associate Editor: E. Arruda. Discussion on the paper should be addressed to the Editor, Prof. Robert M. McMeeking, Journal of Applied Mechanics, Department of Mechanical and Environmental Engineering, University of California—Santa Barbara, Santa Barbara, CA 93106-5070, and will be accepted until four months after final publication of the paper itself in the ASME JOURNAL OF APPLIED MECHANICS.

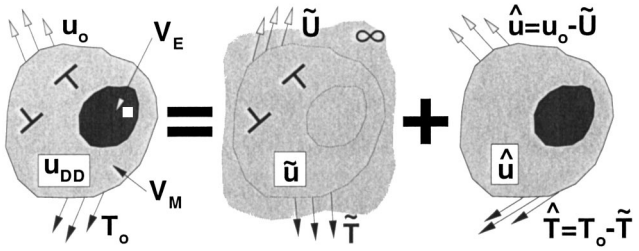

Fig. 1 General discrete dislocation boundary value problem (fields $\mathbf{u}_{DD}$, $\boldsymbol{\sigma}_{DD}$) is written as the superposition of: (i) dislocation fields in infinite space of homogeneous matrix material ($\tilde{\mathbf{u}},\tilde{\boldsymbol{\sigma}}$) and (ii) corrective fields to account for the inclusion and proper boundary conditions ($\hat{\mathbf{u}},\hat{\boldsymbol{\sigma}}$)

ideal for using the DD machinery in a parallel-computing environment. The technique is validated against prior results on two-dimensional (2D) plane-strain crack growth along a rigid/elastic-plastic bimaterial interface, and preliminary results on the fracture of more realistic elastic-plastic/elastic bimaterial interfaces is presented. The superposition formulation and examples discussed will be limited to 2D plane strain. Fundamentally, the technique is equally valid in 3D, although the DD mechanics becomes considerably more complex [15].

The formulation is presented in dyadic notation. Vectors and tensors are given by bold faced symbols, denotes the inner product, and: the trace product. With respect to a Cartesian basis $\mathbf{e}_i$, $\mathbf{a}\cdot\mathbf{b}=a_ib_i$, $\mathbf{A}:\mathbf{B}=A_{ij}B_{ji}$, and $(\boldsymbol{\mathcal{L}}:\mathbf{B})_{ij}=\boldsymbol{\mathcal{L}}_{ijkl}B_{lk}$, with implied summation over repeated indices. Latin indices run from 1 to 3, Greek indices from 1 to 2 only. The gradient operator is denoted as ∇. The fourth-order identity tensor is $\mathcal{I}$.

The remainder of this paper is organized as follows. Section 2 contains a concise overview of the standard DD formulation for inhomogeneous bodies. Section 3 presents the new superposition technique. The material parameters, validation, and preliminary bimaterial results are presented in Section 4. Section 5 discusses other applications of this formulation, and summarizes our results. Computational efficiency for problems involving a nonlinear cohesive zone requires special techniques in the EL subproblem. The Appendix describes an efficient technique for solving the incremental FE equations for an *elastic* bimaterial model with a nonlinear cohesive zone, which is used to solve the EL subproblem in the bimaterial interface crack growth problems.

2 Discrete Dislocation Methodology

The standard DD formulation for the inhomogeneous problem of an elastic-plastic body containing an elastic inclusion has been derived by Van der Giessen and Needleman [7]. The derivation is briefly reviewed here, with a focus on when the implementation becomes computationally expensive. This motivates the development of the new superposition technique, presented in Section 3.

The discrete dislocation formulation models edge dislocations as line defects in an isotropic elastic material, constrained to glide on a fixed slip plane. Long-range dislocation interactions occur through their continuum elastic fields. Short-range interactions are governed by constitutive rules for dislocation motion, nucleation, and annihilation. In addition, dislocations can become pinned at obstacles and are released when the resolved shear stress on the dislocation exceeds the obstacle strength. Nucleation occurs by the expansion of Frank-Read dislocation loops, which in 2D is represented by the creation of a dislocation dipole.

The general discrete dislocation boundary value problem is shown in Fig. 1 for a body of volume V, subject to boundary conditions $\mathbf{u}=\mathbf{u_o}$ on S_u, and $\mathbf{T}=\mathbf{T_o}$ on S_t. The body is composed of an elastic-plastic ''matrix'' region V_M and an elastic ''inclusion'' region V_E with tensors of elastic moduli $\mathcal{L}$ and $\mathcal{L}^E$, respectively. The problem of interest is solved as the superposition of a problem containing dislocations in an infinite body of homogeneous *matrix* material, yielding the displacement, strain, and stress fields $\tilde{\mathbf{u}}$, $\tilde{\boldsymbol{\epsilon}}$, and $\tilde{\boldsymbol{\sigma}}$, and a complementary problem that corrects for the actual boundary conditions and the presence of the inclusion, yielding the fields $\hat{\mathbf{u}}$, $\hat{\boldsymbol{\epsilon}}$, and $\hat{\boldsymbol{\sigma}}$. The fields in the problem of interest are then obtained by superposition as

$$\mathbf{u}_{DD}=\tilde{\mathbf{u}}+\hat{\mathbf{u}} \quad \boldsymbol{\epsilon}_{DD}=\tilde{\boldsymbol{\epsilon}}+\hat{\boldsymbol{\epsilon}} \quad \boldsymbol{\sigma}_{DD}=\tilde{\boldsymbol{\sigma}}+\hat{\boldsymbol{\sigma}} \quad \text{in V} \tag{1}$$

The elastic fields of an isolated dislocation in an infinite body are known analytically [16] and given by $\mathbf{u}^i$, $\boldsymbol{\epsilon}^i$, $\boldsymbol{\sigma}^i$. Again by superposition, the ($\tilde{}$) fields from n_d dislocations are given by

$$\tilde{\mathbf{u}}=\sum_i \mathbf{u}^i \quad \tilde{\boldsymbol{\epsilon}}=\sum_i \boldsymbol{\epsilon}^i \quad \tilde{\boldsymbol{\sigma}}=\sum_i \boldsymbol{\sigma}^i \quad (i=1,\ldots,n_d) \tag{2}$$

These fields produce tractions and displacements at the real boundary of interest given by

$$\begin{aligned} \boldsymbol{\nu}\cdot\tilde{\boldsymbol{\sigma}}&=\tilde{\mathbf{T}} \quad \text{on } S_t \\ \mathbf{u}&=\tilde{\mathbf{U}} \quad \text{on } S_u \end{aligned} \tag{3}$$

where $\boldsymbol{\nu}$ is the outward normal to S.

The corrective field is designed such that when superposed with the infinite space dislocation fields, the desired boundary value problem is obtained. The governing equations for the corrective fields are thus

$$\nabla\cdot\hat{\boldsymbol{\sigma}}=\mathbf{0} \quad \hat{\boldsymbol{\epsilon}}=\nabla\hat{\mathbf{u}} \quad \text{in V} \tag{4}$$

$$\hat{\boldsymbol{\sigma}}=\mathcal{L}:\hat{\boldsymbol{\epsilon}} \quad \text{in } V_M \tag{5}$$

$$\hat{\boldsymbol{\sigma}}=\mathcal{L}^{\mathbf{E}}:\hat{\boldsymbol{\epsilon}}+(\mathcal{L}^{\mathbf{E}}-\mathcal{L}):\tilde{\boldsymbol{\epsilon}} \quad \text{in } V_E \tag{6}$$

subject to the ''corrective'' boundary conditions

$$\begin{aligned} \boldsymbol{\nu}\cdot\hat{\boldsymbol{\sigma}}&=\hat{\mathbf{T}}=\mathbf{T_o}-\tilde{\mathbf{T}} \quad \text{on } S_t \\ \hat{\mathbf{u}}&=\mathbf{u_o}-\tilde{\mathbf{U}} \quad \text{on } S_u \end{aligned} \tag{7}$$

Since the ($\tilde{}$) fields are singular only at the dislocation cores and since dislocations occur in dipole pairs or terminate on traction-free surfaces, the ($\tilde{}$) fields on the boundary S and the boundary conditions (7) for the corrective field problem are smooth, and thus the corrective field problem can be solved with the conventional FE method.

With the dislocation structure and all fields known at some instant, the evolved structure and fields are desired after an increment in applied loading. Based on the known dislocation structure, the boundary fields $\tilde{\mathbf{U}}$ and $\tilde{\mathbf{T}}$ are calculated. The corrective FE problem is then solved for an increment of applied loading. With the total fields determined, the evolution of the dislocation structure is accomplished by i) evaluation of the Peach-Koehler force on each dislocation and ii) application of the rules for dislocation motion, nucleation, and annihilation. The updated dislocation structure and new fields are now known, and this procedure is repeated for all subsequent increments. The Peach-Koehler force $f^{(I)}$ on the Ith dislocation is computed as

$$f^{(I)}=n_i^{(I)}\left(\hat{\sigma}_{ij}+\sum_{J\neq I}\sigma_{ij}^{(J)}\right)b_j^{(I)} \tag{8}$$

where $n_i^{(I)}$ is the slip plane normal and $b_i^{(I)}$ is the Burgers vector of the Ith dislocation. A key point is that the method does not solve for equilibrium dislocation distributions. The dislocation velocity is linearly related to the Peach-Koehler force; no dissipative mechanism to slow the dislocations is included. At any instant, the dislocation structure is a snapshot of the constantly evolving dislocation structure. Since an equilibrium solution is not being sought, no self-consistent iteration between the two subproblems is necessary. The FE framework used here is that of Cleveringa et al. [9], which is quasi-static and uses a virtual work expansion to step forward in time without iteration.

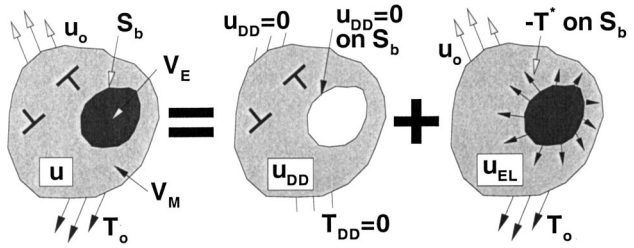

Fig. 2 New superposition framework showing decomposition into two subsidiary problems: discrete dislocation (DD) subproblem solved with the standard formulation subject to generic boundary conditions, and elastic (EL) subproblem, which contains all specific boundary conditions and loading, solved with standard elastic FE

The additional term $\hat{\mathbf{p}}=(\mathcal{L}^{\mathbf{E}}-\mathcal{L}):\tilde{\boldsymbol{\epsilon}}=(\mathcal{L}^{\mathbf{E}}:\mathcal{L}^{-1}-\mathcal{I}):\tilde{\boldsymbol{\sigma}}$ in Eq. (6) that corrects for the presence of the inclusion is known as the polarization stress. In an incremental FE scheme the polarization stress must be computed at each inclusion integration point, which requires the stress field of each dislocation to be evaluated at these points. This is a major computational limitation when applying the DD method to elastically inhomogeneous structures. As the number of dislocations becomes large and/or the number of inclusion elements increases, evaluation of $\hat{\mathbf{p}}$ can dominate the FE calculation. For this reason most of the DD literature has focused on homogeneous materials. This motivates our development of a new DD technique.

3 Superposition Method for DD Plasticity

The new superposition technique is shown schematically in Fig. 2. The general problem is exactly the same as in Fig. 1, however, a different decomposition is used. The desired boundary value problem is solved as the superposition of a DD subproblem subject to generic boundary conditions and a fully elastic (EL) subproblem subject to all actual boundary conditions.

The DD subproblem models only that part of the structure where dislocations are permitted to exist; the regions of elastic inhomogeneity are not modeled in the DD subproblem. The generic boundary conditions of the DD subproblem are chosen as $\mathbf{u}_{DD}=\mathbf{0}$ and $\mathbf{T}_{DD}=\mathbf{0}$ on S_u and S_t, respectively. Additionally $\mathbf{u}_{DD}=\mathbf{0}$ is prescribed on the boundary S_b between the matrix and inclusion. Thus, the only information about the full problem that is used in the solution of the DD subproblem is the geometry of the plastic region and the knowledge of whether displacement or traction boundary conditions are applied on boundaries shared by the DD subproblem and the full problem. The incremental solution of the DD subproblem is then obtained exactly as described in the previous section, i.e., as the superposition of an infinite space dislocation problem and a corrective problem. An outcome of the solution of the DD subproblem at any instant is a traction $\mathbf{T}^*$ along the boundary S_b, which is used in the EL subproblem as described below.

The EL subproblem models the entire structure and is subject to all the true boundary conditions on S. The region of the structure containing dislocations is modeled as an isotropic elastic material. Information about the plastic deformation in the plastic region of the material is transmitted to the remainder of the structure through the addition of a body force $-\mathbf{T}^*$ along S_b in the EL subproblem, which is the negative of the traction $\mathbf{T}^*$ obtained from the DD subproblem. The EL subproblem can be solved by standard FE methods. In the absence of nonlinear regions, such as a cohesive zone surface, the EL subproblem is fully linear and the FE equations can thus be solved very quickly because inversion or decomposition of the entire elastic stiffness matrix must be accomplished only once at the start of the calculation.

The solution to the full problem of interest is then obtained by superposition of the DD and EL subproblems as

$$\mathbf{u}=\mathbf{u}_{DD}+\mathbf{u}_{EL} \quad \boldsymbol{\epsilon}=\boldsymbol{\epsilon}_{DD}+\boldsymbol{\epsilon}_{EL} \quad \boldsymbol{\sigma}=\boldsymbol{\sigma}_{DD}+\boldsymbol{\sigma}_{EL} \tag{9}$$

Superposition is permitted since, in the region where superposition is being used, both problems are linearly elastic at any instant. All plasticity is completely contained in the motion and position of the dislocations within the underlying elastic material and, therefore, does not preclude the application of superposition. Although termed an ''elastic'' subproblem, the EL subproblem need only be linear in the region where the discrete dislocation superposition is being applied. That superposition yields the correct boundary conditions for the desired problem during any increment is clear from the schematic in Fig. 2: the boundary conditions are satisfied exactly, the linear field equations in each part of the problem have been solved via FEM, the tractions $\mathbf{T}^*$ and $-\mathbf{T}^*$ cancel upon superposition, and the boundary condition $\mathbf{u}_{DD}=\mathbf{0}$ has no effect on the displacement of the boundary S_b as calculated in the elastic subproblem.

The EL subproblem influences the dislocation structure and its evolution because the Peach-Koehler force is calculated on each dislocation using the full field $\boldsymbol{\sigma}$ minus the dislocation self-interaction, which thus includes the contribution $\boldsymbol{\sigma}_{EL}$. In all applications, it must be remembered that the dislocations are driven by the full, true field and not simply the fields $\boldsymbol{\sigma}_{DD}$ calculated in the DD subproblem. The expression for the Peach-Koehler force in this superposition framework is

$$f^{(I)}=n_i^{(I)}\left(\hat{\sigma}_{ij}+\sum_{J\neq I}\sigma_{ij}^{(J)}+\sigma_{ij}^{EL}\right)b_j^{(I)} \tag{10}$$

which differs from the corresponding expression for the standard formulation (8) by the inclusion of the $\boldsymbol{\sigma}_{EL}$ contribution.

Before proceeding to validate and use the new superposition method, some comments are warranted. Operationally, at each increment the new superposition method requires two FE calculations: one for the corrective fields in the DD subproblem and one for the entire EL subproblem. The overall DD subproblem is solved with standard DD machinery (described in Section 2), and as the region is elastically homogeneous, there are no polarization stresses. The new superposition method is thus advantageous in elastically inhomogeneous problems with large numbers of dislocations and/or many inclusion elements. The calculation of $\hat{\mathbf{p}}$ is eliminated at the cost of an additional FE calculation for the EL subproblem.

The DD subproblem is largely independent of the particular problem under study. Aside from adding the field $\boldsymbol{\sigma}_{EL}$ to drive the dislocations, the DD subproblem may know nothing, or only little, about the actual problem (geometry and loading) under study. If the plastic zone of the problem is constrained to occur within a finite region of space, then the DD problem can be further confined within that box, with no knowledge whatsoever about the full geometry. In this sense, the DD subproblem serves as a ''black-box'' constitutive material law for the plastic flow of the plastically deforming material. The DD subproblem is, however, limited to small strains.

Because the DD subproblem is largely disconnected from the actual problem of interest, the decomposition of the problem also provides opportunities for parallel coding for a wide variety of problems, as will be discussed further in Section 5.

4 Application to Bimaterial Interface Fracture

Crack growth in plastically deforming materials is an attractive application of the DD methodology. It is well known that in continuum plasticity the maximum opening stress ahead of the crack tip is, at most, about five times the yield strength. Such low near-tip stresses are unable to cause crack growth in many cases involving nonductile fracture modes. Furthermore, for brittlelike fracture occurring by cleavage of atomic planes, the fracture process zone is small (nanoscale), and the peak stresses required for

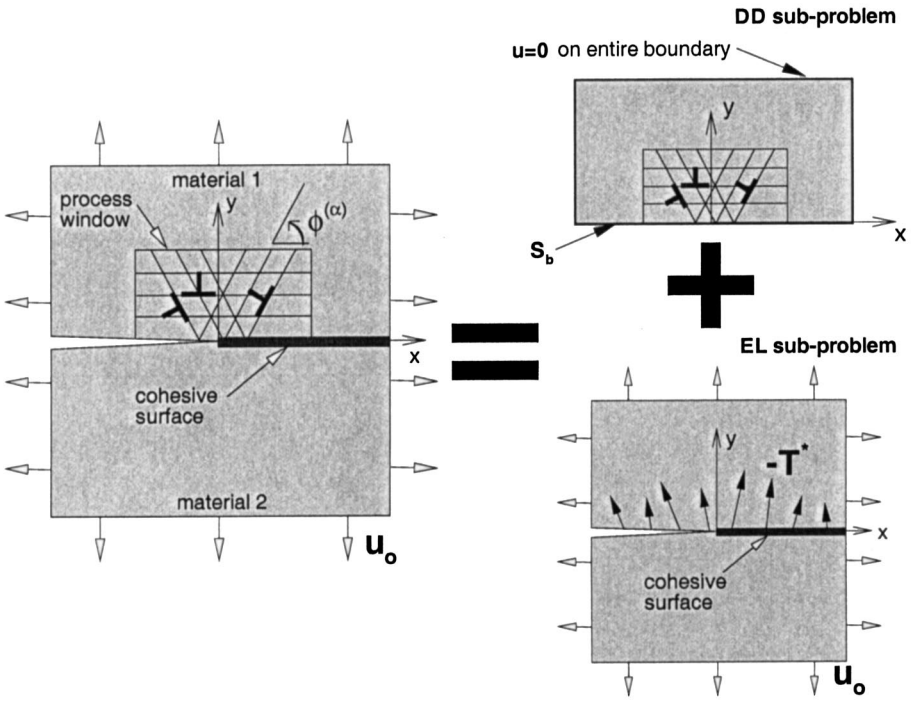

Fig. 3 Decomposition of the bimaterial fracture problem into DD and EL subproblems

material separation are large. Continuum plasticity is not expected to handle the high local stresses and stress gradients prevailing around the crack tip in such situations. Cleveringa et al. [9] thus applied the DD methodology to crack growth in a homogeneous elastic-plastic material and predicted R-curve behavior for the onset of crack growth. Their results demonstrated that dislocation organization on the scale of microns can generate the high stresses needed to grow the crack. On the other hand, the dislocation structures also generated stress fields away from the crack tip that were in generally good agreement with the continuum fields predicted by using a perfectly plastic constitutive law.

The bimaterial interface fracture problem is also suited toward treatment via the DD methodology for similar reasons. At the continuum level, the fields around a semi-infinite interface crack separating two dissimilar *elastic* half spaces were given by Rice [17]. More recently Tvergaard and Hutchinson [18–20] and Tvergaard [21–23] have explored the effects of plasticity in one or both materials. Tvergaard [23] has shown that for an elastic-plastic/elastic bimaterial, the toughness increases with increasing modulus of the purely elastic material. When the purely elastic material is at least twice as stiff as the elastic-plastic material, fracture is largely suppressed when the peak cohesive strength is roughly four times the yield stress [23]. This is expected since the cohesive strength approaches the maximum possible opening stress of the continuum model. Continuum models have been augmented by additional assumptions about the near-tip behavior. Thus Tvergaard [21,22] modeled brittle fracture with the dislocation free zone (DFZ) model of Suo et al. [24]. The DFZ model for cleavage crack growth assumes that the crack tip does not emit dislocations, stays nanoscopically sharp, and is surrounded by a thin *elastic* strip with the far-field region governed by continuum plasticity. The elastic singular field gives rise to high near tip stresses and plastic flow provides dissipation. Fracture in the elastic strip region is governed by linear elastic fracture mechanics (LEFM); crack growth is characterized by a critical stress intensity at the crack tip. The DD model, in contrast, makes no assumptions about a dislocation free region, but such a region may emerge naturally from the solution to the boundary value problem, providing insight into the size and evolution of the dislocation free region. Furthermore, fracture is an outcome of the DD solution and does not require any a priori modeling changes.

The elastic-plastic/elastic bimaterial interface problem and its decomposition using our superposition framework are shown schematically in Fig. 3. Two materials, an elastic-plastic upper half-space and an elastic lower half-space are separated by an interface that is described by a cohesive zone model (CZM). The overall material is loaded by displacements corresponding to the desired elastic K-field (see below). Far to the left, the cohesive zone is fully open and the crack surfaces are traction free. Far to the right, the cohesive zone is essentially closed and the displacements are continuous across the interface. Due to the existence of the cohesive zone, there is no crack-tip singularity in this problem. In decomposing this problem, the DD subproblem is used to model the elastic-plastic upper half plane and the EL subproblem models the entire body as an elastic/CZM problem. The boundary S_b is taken to be the entire lower boundary of the DD subproblem, i.e., the entire upper crack surface in the EL subproblem. This choice gives a smooth traction $\mathbf{T}^*$ along the entire boundary S_b that is exported to the EL subproblem. Choosing a more traditional crack boundary condition of zero traction along the open crack and zero displacement along the originally closed crack would yield a singularity in the traction $\mathbf{T}^*$ at the original crack tip in the DD subproblem. This would be difficult to resolve and handle properly in the superposition framework. The latter boundary conditions would also unnecessarily bias the entire problem toward the original crack tip.

As the bimaterial specimen is loaded, dislocations generated in the plastic material may pass out of the traction-free and/or partially open regions of the cohesive surface. This behavior is entirely physical, as the surface and cohesive zone in regions where its stiffness is becoming small, absorb the dislocations. The occurrence of this phenomenon in the new superposition technique requires comment. The DD subproblem contains all the dislocations, but subject to the boundary condition $\mathbf{u}_{DD}=\mathbf{0}$ everywhere. However, the Peach-Koehler force on a dislocation is always evaluated using the *total* fields, and hence, the dislocations move,

correctly, as if in the full problem. The zero displacement boundary condition imposed in the DD subproblem is not actually seen by the dislocations. Thus, a dislocation can experience a driving force to move it out of the DD subproblem domain through the surface S_b. Physically, this leaves a step having magnitude of the Burger's vector along S_b. In terms of the DD superposition of Fig. 1, the $\tilde{\mathbf{u}}$ displacement field has a step where the dislocation exited the surface (due to the existence of the other half of the dislocation dipole that remains inside the material). Recalling Eq. (1), to satisfy the imposed $\mathbf{u}_{DD}=\mathbf{0}$ constraint on S_b, the $\hat{\mathbf{u}}$ corrective field must have an equal and opposite step at the same point on S_b. Thus, the DD subproblem of Fig. 3 is no longer smooth, and there is a singularity in the traction $\mathbf{T}^*$ at the point along S_b where the dislocation has passed through. It is not possible to accurately resolve the $\mathbf{T}^*$ singularities associated with dislocation surface steps on S_b, but an exact resolution is *not* required. If identical meshes are employed in the overlapping regions of the EL and DD subproblems, which is also desirable for other reasons, then the *approximate*, *nonsingular* FE traction $\mathbf{T}^*$ in the DD subproblem is exactly cancelled by the field $-\mathbf{T}^*$ applied in the EL subproblem. The field $-\mathbf{T}^*$ in the EL subproblem creates the physical surface step in the problem, resolved to the accuracy of the FE mesh. In other words, part of the traction $\mathbf{T}^*$ in the DD subproblem serves to generate an elastic field to *eliminate* the surface step, and the step is then *recreated* by the application of $-\mathbf{T}^*$ in the EL subproblem. Comparison of the new superposition technique to the standard DD method below shows that the surface steps are handled precisely via the superposition.

4.1 Model Parameters and Loading. The results presented here are based on the geometry and dislocation parameters previously used by Cleveringa et al. and Deshpande et al. [9,10] to study mode I and fatigue crack growth, respectively. In fact, we have used the actual code of Deshpande et al. [10], modified to include $\boldsymbol{\sigma}_{EL}$ from the EL subproblem to the P-K force, thus treating the entire DD code as a "black-box." We consider a specimen of 1000×1000 μm, and take the origin of an xy-coordinate system to be at the center of the sample. The initial crack tip is located at the origin and assumed to be open ($\mathbf{T}=\mathbf{0}$) for $y=0$, $x<0$ and a cohesive zone describes the interface properties for $y=0$, $x>0$. The sample is meshed with 120×220 bilinear quadrilateral elements; displacement boundary conditions correspond to an applied remote K field. The properties of the metal, i.e., the elastic-plastic upper half plane ($y>0$), are consistent with Aluminum ($E_1=70$ GPa, $\nu_1=0.33$). The elastic modulus E_2 of the ceramic ($y<0$) will be varied (with $\nu_2=0.33$). Dislocation activity in the upper half plane is restricted to a 15×15 μm "process window" of 80×80 elements, graded around the crack tip. The slip plane geometry is representative of an FCC type single crystal, with three slip systems oriented at $+60°$, $-60°$, and $0°$ relative to the crack plane $y=0$, spaced at $100b$ and initially dislocation-free. Only edge dislocations are considered, with Burgers vector of magnitude $b=0.25$ nm. The dislocation glide velocity is linear in the Peach-Koehler force with viscous drag coefficient $B=10^{-4}$ Pa s, and climb is not permitted. Dislocation nucleation occurs by the expansion of Frank-Read sources, randomly dispersed in the process window with density $\rho_{nuc}=66/\mu\text{m}^2$. Nucleation occurs when the Peach-Koehler force at a source exceeds a critical value of $\tau_{nuc}b$ for a time period of $t_{nuc}=10$ ns. The value of τ_{nuc} is chosen from a Gaussian distribution with mean strength $\overline{\tau}_{nuc}=50$ MPa and standard deviation $0.2\overline{\tau}_{nuc}$. Dislocations of opposite sign are annihilated when they come within a critical distance of $6b$. The process window also contains a random distribution of obstacles with density $\rho_{obs}=170/\mu\text{m}^2$ that pin dislocations until the Peach-Koehler force reaches the obstacle strength $\tau_{obs}=150$ MPa. To fully resolve the dislocation activity a time step of $\Delta t=0.5$ ns was used, which necessitates the use of a high loading rate of $\dot{K}=100\ \text{GPa m}^{1/2}/\text{s}$. Since an iterative numerical scheme is not used, the time step is not chosen from stability considerations. Instead the time step must be small enough to resolve t_{nuc}, which is the intrinsic time scale of the problem.

In the EL subproblem, we use the coupled normal-shear cohesive law relating the displacement jump $\boldsymbol{\Delta}$ across the interface to the traction $\mathbf{T}$ introduced by Xu and Needleman [25]. The tractions are obtained from a potential ϕ as $\mathbf{T}=\partial\phi/\partial\boldsymbol{\Delta}$, with

$$\phi=\phi_n+\phi_n\exp\left(-\frac{\Delta_n}{\delta_n}\right)\left\{\left[1-r+\frac{\Delta_n}{\delta_n}\right]\frac{1-q}{r-1}-\left[q+\left(\frac{r-q}{r-1}\right)\frac{\Delta_n}{\delta_n}\right]\exp\left(-\frac{\Delta_t^2}{\delta_t^2}\right)\right\} \tag{11}$$

where δ_n and δ_t are the normal and tangential characteristic lengths, respectively, and the work of normal and tangential separation are

$$\phi_n=e\,\sigma_{\max}\delta_n,\quad \phi_t=\tau_{\max}\delta_t\sqrt{\frac{e}{2}}$$

where $\sigma_{\max}$ and $\tau_{\max}$ are the normal and shear cohesive strengths, respectively. The normal-shear coupling is included through parameters

$$q=\frac{\phi_t}{\phi_n},\quad r=\frac{\Delta_n^*}{\delta_n}$$

where Δ_n^* is the value of Δ_n after a complete shear separation with $T_n=0$. The characteristic lengths are taken to be $\delta_n=\delta_t=0.5$ nm, and the interface strengths are $\sigma_{\max}=0.3$ GPa and $\tau_{\max}=0.699$ GPa. Then $\phi_n=\phi_t=0.408\ \text{J m}^{-2}$, giving $q=1$. The parameter r is taken to be zero.

Assuming small-scale yielding, the remote boundary conditions are characterized by the bimaterial elastic K-field. The displacement field for the upper half plane is [19]

$$u_1+\mathrm{i}u_2=\frac{|K|}{2\mu_1\cosh(\pi\epsilon)}\sqrt{\frac{R}{2\pi}}\left\{\frac{(3-4\nu_1)\mathrm{e}^{\mathrm{i}\theta/2+\epsilon(\theta-\pi)-\mathrm{i}\bar{\psi}}}{1-2\mathrm{i}\epsilon}-\frac{\mathrm{e}^{-\mathrm{i}\theta/2-\epsilon(\theta-\pi)-\mathrm{i}\bar{\psi}}}{1-2\mathrm{i}\epsilon}-\mathrm{i}\sin\theta\,\mathrm{e}^{\mathrm{i}\theta/2+\epsilon(\theta+\pi)+\mathrm{i}\bar{\psi}}\right\} \tag{12}$$

where $K=K_1+\mathrm{i}K_2$, and $R=\sqrt{x^2+y^2}$. The form for the lower half plane is similar. The elastic mismatch is included through ϵ, given as

$$\epsilon=\frac{1}{2\pi}\ln\left(\frac{1-\beta}{1+\beta}\right)$$

where

$$\beta=\frac{1}{2}\frac{\mu_1(1-2\nu_2)-\mu_2(1-2\nu_1)}{\mu_1(1-\nu_2)+\mu_2(1-\nu_1)}$$

The mode mixity is described by a phase angle ψ such that

$$\tan\psi=\frac{\mathrm{Im}[(K_1+\mathrm{i}K_2)L^{\mathrm{i}\epsilon}]}{\mathrm{Re}[(K_1+\mathrm{i}K_2)L^{\mathrm{i}\epsilon}]} \tag{13}$$

where L is a reference length used to characterize the remote field and $\bar{\psi}$ varies with r as

$$\bar{\psi}=\psi+\epsilon\ln(r/L) \tag{14}$$

The remote loading is thus characterized by $|K|$, ψ, and L. Physically, ψ measures the ratio of shear to normal stress on the interface a distance L from the tip, as predicted by the elastic solution [19]. We take $L=10$ μm, which is on the order of the process window size. Tvergaard [23] defines a reference stress intensity factor

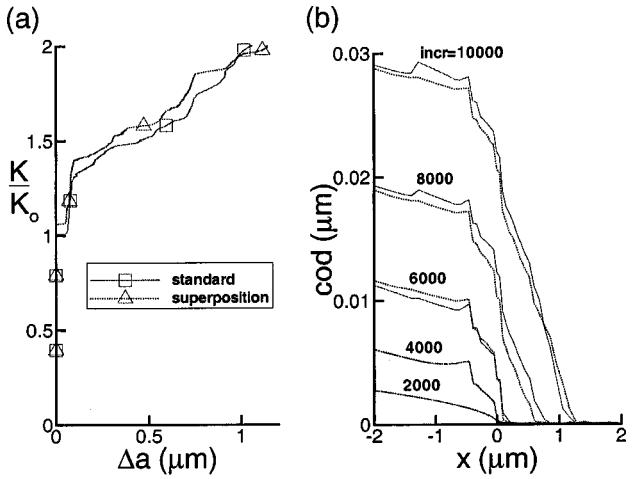

Fig. 4 Comparison of superposition and standard DD methods for rigid substrate: (a) crack growth resistance curves and (b) crack opening displacements

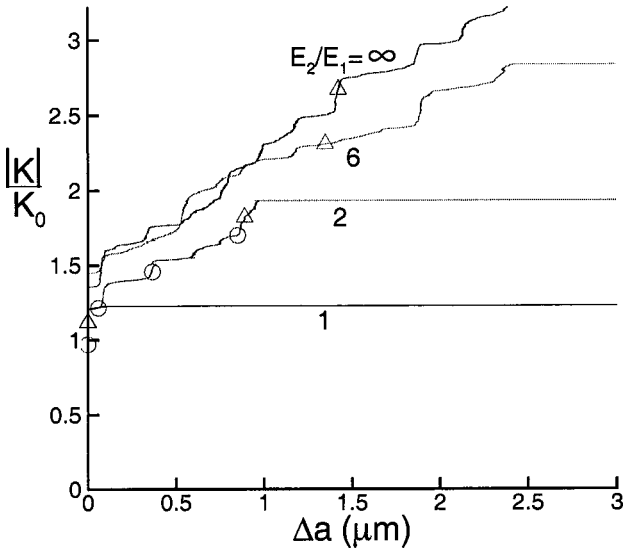

Fig. 5 Normalized applied stress intensity factor $|K|/K_0$ versus crack extension Δa for various substrate moduli

$$K_0=\left[\frac{1-\nu_1^2}{E_1}+\frac{1-\nu_2^2}{E_2}\right]^{-1/2}\left(\frac{2\Gamma_o}{1-\beta^2}\right)^{1/2} \tag{15}$$

where Γ_o is the work of separation of a mode-independent cohesive law. With $q=1$ (as is the case here), the cohesive law (11) is mode-independent, thus we set $\Gamma_o=\phi_n=\phi_t$ in (15) to calculate the reference K_0.

4.2 Validation. The superposition technique was validated by comparing to existing results obtained with the standard DD method for the problem of an elastic-plastic half-space on a rigid substrate. Use of a rigid substrate permits the DD problem to be solved only in the upper half-space, so that the standard method is appropriate and efficient. In both cases, exactly the same material was modeled, i.e., the exact same random distribution of sources and obstacles was used for both methods. Figure 4 shows the crack growth resistance curve and the evolution of the crack opening displacement with load level as obtained from the standard method and the superposition method. Excellent agreement in both quantities is obtained. Due to the chaotic nature of the discrete dislocation simulations, as discussed by Deshpande et al. [26], the fields are expected to agree within 10%. The variations in the R-curves are well within the range of chaotic effects. It is worth noting the excellent agreement in the crack surface features associated with dislocations exiting through the crack surface as the deformation proceeds. Simpler problems involving single dislocation sources are essentially exactly reproduced. These results fully validate the superposition technique and its numerical implementation. The superposition technique, including the treatment of dislocations passing through surfaces with fixed displacement boundaries of the DD subproblem, can thus be extended to the analysis of new problems with confidence.

4.3 Results. Here we present some preliminary results on the fracture toughness versus elastic mismatch for a bimaterial interface. The experimental results of Liechti and Chai [27] and the simulations of Tvergaard [23] both demonstrate a strong dependence of the R-curve on the elastic mismatch and phase angle of the applied loading, with significantly less-tough behavior found for modest ratios of elastic mismatch E_2/E_1 as compared to the rigid substrate case. Thus, the standard DD method for the rigid substrate problem is expected to greatly overpredict toughness relative to realistic metal/ceramic systems and cannot be extended to realistic systems without high computational cost.

Figure 5 shows the crack growth resistance curves for bimaterial specimens of Aluminum, as modeled above, on substrates of varying elastic modulus. The ratio of $E_2/E_1=6$ corresponds roughly to Aluminum on SiC, while the ratio $E_2/E_1=2$ corresponds to Aluminum on Si. With increasing stiffness ratio, the bimaterial interface shows a rapidly increasing toughness. For the $E_2/E_1=\infty$ specimen the simulation was stopped before a failure point was reached. Figure 6 shows the opening stress σ_{22} and dislocation positions at a load near the failure point for $E_2/E_1=1$, 2, and 6, and at a high load for the $E_2/E_1=\infty$ specimen. When $E_2/E_1=1$ relatively few dislocations are nucleated, the crack remains sharp, and fracture occurs in an almost entirely brittle manner, with negligible toughening. That failure occurs at $|K|/K_0>1$ is due to the neglect of the shear toughness of the interface in choosing the reference K_0 [see comments after Eq. (15)]. The other R-curves all exhibit regimes of toughening and spurts of brittle crack extension. The periods where a large increase in $|K|$ occurs over a small Δa correspond to the crack tip field repeatedly activating one (or several) nearby sources. Crack blunting follows as one dislocation of a dipole pair passes out of the crack surface, while the other slips away from the crack surface into the material. Eventually the dislocations in the material provide a backstress sufficient to shut down the source(s) or a near-tip dislocation configuration generates high stresses resulting in a spurt of crack growth. This semi-brittle extension occurs with a relatively small increase in applied $|K|$. This brittle extension is either stopped when the new crack tip field activates other nearby sources, or if sufficiently weak sources are not nearby and/or the crack is growing very rapidly the extension continues and the specimen fails. When comparing the R-curves of Fig. 5 it is worth noting that since the applied loading was defined by $\psi=0$ at $L=10\,\mu$m the variation in substrate modulus results in varying amounts of shear closer to the crack tip. The variation of phase along the interface is particular to the inhomogeneous crack problem, and such mixed mode effects will be examined in detail in a future publication.

The evolution of the opening stress and dislocation structure for the $E_2/E_1=2$ specimen are shown in Fig. 7. In Fig. 7(*a*) at $|K|/K_0=0.966$ the crack tip is sharp and very few dislocations have been nucleated. When $|K|/K_0=1.208$ the majority of the slip is occurring on two slip planes with $+60°$ orientation. As one dipole slips into the material, the other glides toward the crack tip, passes out, and blunts the crack. As loading continues, additional sources become activated; at $|K|/K_0=1.449$ one or two $-60°$ slip planes have a cluster of dislocations near the initial crack tip. At $|K|/K_0=1.691$ the crack has extended roughly 0.85 μm and new

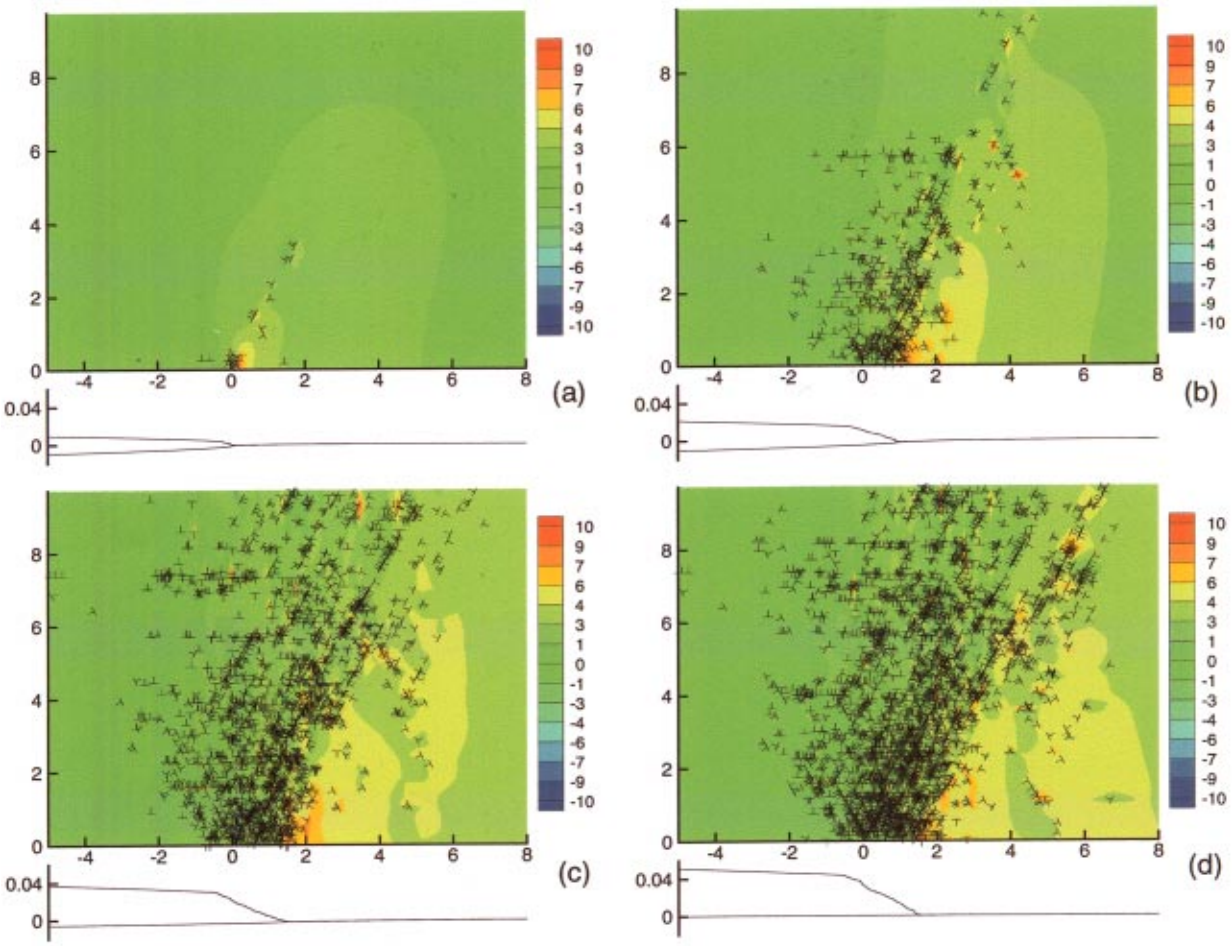

Fig. 6 (Color online) Dislocations and normalized opening stress $\sigma_{22}/\mu\times10^3$ in a 10×13 μm region near the crack tip for various substrate moduli just prior to failure (see triangles in Fig. 5): (a) $E_2/E_1=1$ with $|K|/K_0=1.118$, (b) $E_2/E_1=2$ with $|K|/K_0=1.811$, (c) $E_2/E_1=6$ with $|K|/K_0=2.304$, and (d) $E_2/E_1=\infty$ with $|K|/K_0=2.286$. The crack opening profiles for each case are plotted below the *x* axis. All distances are in microns.

sources are activated. A snapshot just before failure of this specimen is shown in Fig. 6(*b*) where $|K|/K_0=1.811$.

The model DD parameters used for Aluminum generate a yield stress of about 60 MPa [28]. As discussed above, the normal cohesive strength is 300 MPa, thus $\sigma_{\max}/\sigma_y=5$. In the continuum models of Tvergaard [23], such a large ratio of cohesive strength to yield stress essentially precludes crack growth, except when the substrate is very soft ($E_2/E_1=1$). In the DD model, however, brittle fracture is reached in all cases except that for the rigid substrate, as seen in Fig. 5. This highlights the dual role of dislocations in elastic-plastic fracture: the motion and interaction of dislocations provides dissipation and increased toughness, but the dislocations also generate local stresses reaching the cohesive strength and thus driving crack growth. The latter effect is missing in standard continuum simulations. Qualitatively, however, the R-curves found here do agree with those found by Tvergaard at a lower ratio of $\sigma_{\max}/\sigma_y=3$ (Fig. 4. in [23]).

The trend of increasing toughness with increasing substrate modulus can be justified by the following qualitative analysis. The work of the applied loading is apportioned between the elastic deformations of the substrate and plastic material and the dissipation due to plastic flow. The plastic flow itself is driven by the stresses, and hence stored work, in the plastic material. Thus, with increasing rigidity of the substrate, more work is put into the plastic material and a larger fraction of that work is dissipated by plastic flow. In the rigid limit, all of the deformation and stored elastic energy resides in the plastic material, and the deformation drives a high degree of plastic dissipation and, hence, a high overall toughness. As the substrate becomes very soft, all of the energy is stored in the deformation of the substrate, preempting plastic flow and dissipation in the plastic material and causing completely brittle fracture.

The preliminary DD results can provide insight into the relevance or necessity of the dislocation free zone concept to bimaterials. Excluding the $E_2/E_1=1$ specimen, which has such few dislocations that it exhibits almost completely brittle fracture, there is no consistent observation of a DFZ throughout the load history. When $E_2/E_1=2$ a strip approximately 0.1 μm from the *free* crack surface does not contain dislocations (see Fig. 7). This is expected as nearby dislocations (on a $\pm60°$ plane) will be attracted to the free surface and pass out. However, for the $E_2/E_1=2$, 6, ∞ ratios, particularly at elevated loading, a DFZ is not observed down to the resolution of this analysis (see Fig. 7); the minimum near-tip element size is 0.05 μm and the intrinsic cohesive length scale $\delta_c(=\sigma_{\max}\delta_n/E)$ for the problem is 0.11 μm and so ''crack-tip'' phenomena are not resolved below this scale. In addition, the crack profiles in Figs. 6 and 7 all exhibit significant blunting before failure, which is inconsistent with the DFZ assumption of a nanoscopically sharp crack. However, the preliminary DD results suggest that crack growth is due primarily to high near-tip stresses, resulting from the applied load and near-tip dislocation structures, and not the blunting of the crack as the cohe-

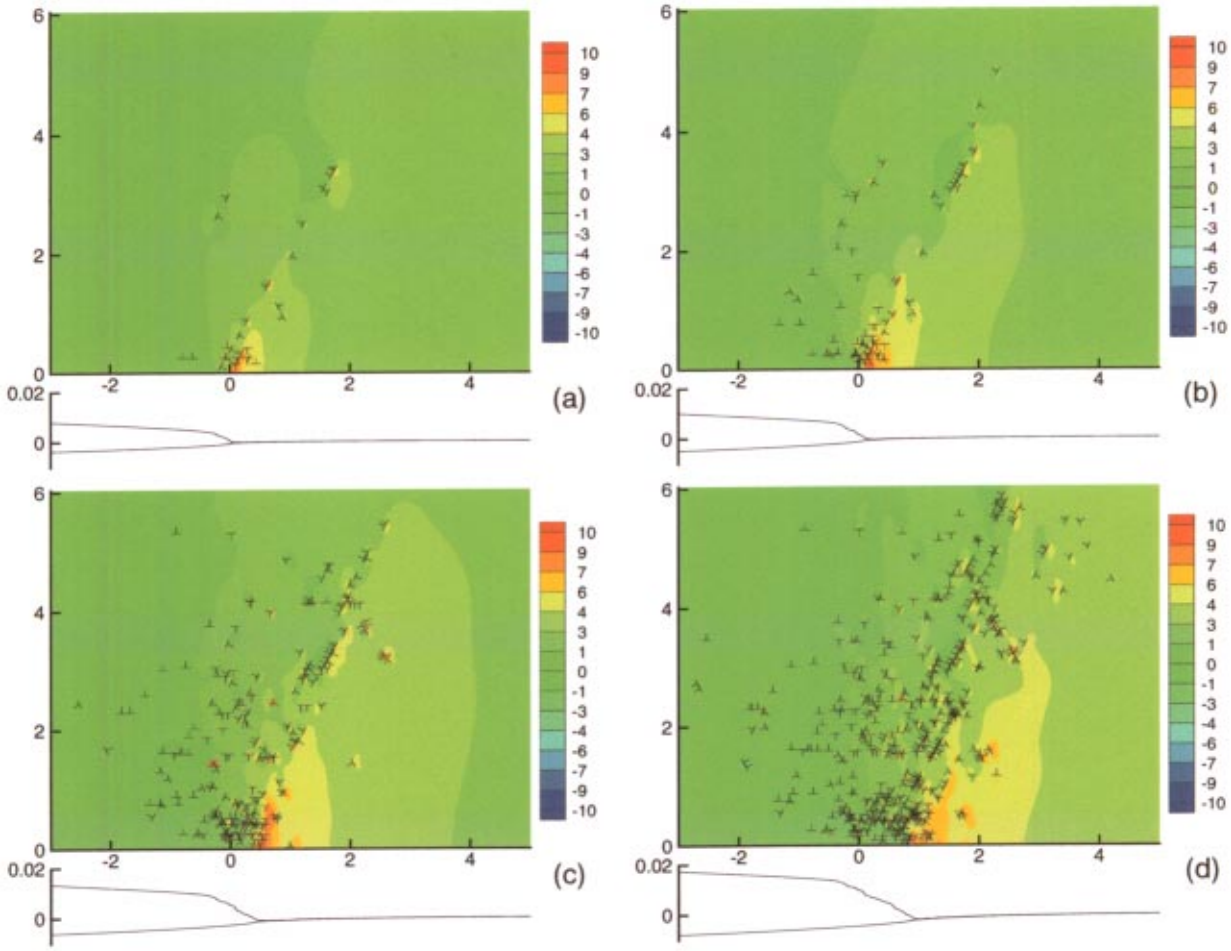

Fig. 7 (Color online) Dislocations and normalized opening stress $\sigma_{22}/\mu\times10^3$ in a 8×6 μm region near the crack tip for $E_2/E_1=2$ at four stages of loading (see circles in Fig. 5): (a) $|K|/K_0=0.966$, (b) 1.208, (c) 1.449, and (d) 1.691. The crack opening profiles at each load are plotted below the x axis. All distances are in microns.

sive zone absorbs dislocations. The results here also support the observation of Wei and Hutchinson [29] that even when a DFZ is appropriate, it may be so small that a nonlocal plasticity theory is required to match to the large gradients present in the elastic DFZ strip.

This represents a preliminary overview of the elastic-plastic/elastic bimaterial problem. A much more detailed analysis will be performed in a future publication, including examination of the influences of i) cohesive law details (e.g., shear versus normal strengths and shear/normal coupling); ii) the ratio of the cohesive strength to yield stress; and iii) mode mixity of the remote loading, an analysis of the underlying dislocation structures and their relationships to observed trends, and a study of statistical effects.

5 Discussion and Conclusions

We have presented a general new technique for the efficient extension of the DD plasticity method to problems with elastic inhomogeneities. The usefulness of the method lies in its isolation of the DD part of the model from many of the particular features of the problem under consideration. The DD calculation only requires information about the geometry of the region where dislocations may be present, and is supplied, via the superposition, with driving forces on the dislocations coming from the elastic subproblem. This construction effectively allows for the use DD plasticity as a ''black-box'' constitutive input in any desired region.

The existing DD method involves continuum representations of many atomistic phenomena, including nucleation, glide, pinning, and annihilation. Work is currently in progress on incorporating additional physical features of dislocation behavior (i.e., junctions, source generation, and stage II hardening) into the 2D formulation [30]. The superposition technique can assimilate any such changes without difficulty because it is unaffected by any of the inner workings of the DD method.

The superposition method can also be used to handle problems containing multiple plastic domains. In such problems, each plastic domain requires its own DD calculation and generates tractions $\mathbf{T}^*$ on the relevant surfaces S_b that are incorporated into the single EL subproblem. Upon solution of the full EL subproblem, the stress fields are exported back to the DD calculations in each domain. Some physical applications of this approach are to metal/ceramic multilayers, polycrystalline structures (each grain treated separately, see Fig. 8), and layered metal/metal structures where variations in elastic and plastic properties exist from layer to layer. For the polycrystalline structure of Fig. 8 a separate DD subproblem is constructed for each grain. The tractions T^* in the EL subproblem are calculated at the appropriate boundaries in the DD subproblem; boundaries common to two grains will have T^* contributions from each grain.

The superposition method also serves as a basis for parallel computations. The DD problem(s) can be divided into any number of subregions, either for physical or mathematical convenience. Each subvolume DD calculation requires only the calculation of

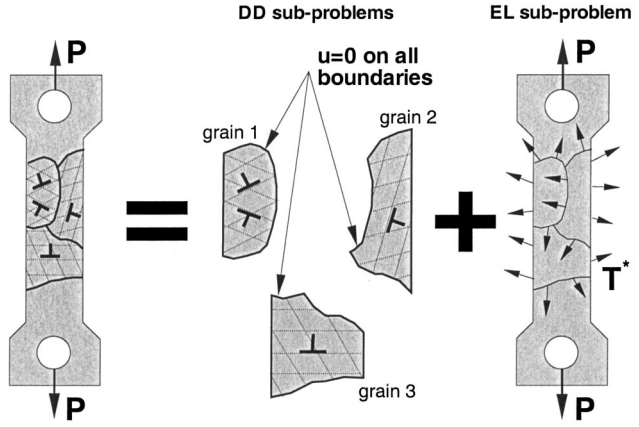

Fig. 8 Schematic of the superposition technique applied to a 2D polycrystalline structure. Each DD problem is independent and thus the computation is easily parallelized.

dislocation/dislocation interactions within that volume. All other dislocation interactions are fully accounted for through the external (EL sub-problem) fields and exported tractions. Since each subvolume DD calculation is self-contained, these calculations can be performed independently and simultaneously on separate processors. For instance, for the polycrystalline model in Fig. 8 each grain can be handled simultaneously on a separate processor. Dislocations passing from one subvolume to another are handled seamlessly just as we have treated dislocations passing through a cohesive surface in the bimaterial problem.

In conclusion, the DD model allows, in principle, for the study of numerous problems where the characteristic dimensions are on the order of tens of microns, at which scales continuum plasticity is unable to reproduce observed size effects. The new DD superposition technique developed here extends the practical range of application of the DD method to problems with elastic inhomogeneities, multiple plastic domains, and larger physical sizes. Preliminary application to bimaterial interface cracking shows the power and generality of the approach. Future work will address the detailed analysis of crack growth along bimaterial interfaces as well as other problems to which the general DD approach is well suited.

Acknowledgments

The authors gratefully acknowledge the support of this work by U.S. Air Force Office of Scientific Research through the MURI program ''Virtual design and testing on materials: A multiscale approach,'' Grant No. F49620-99-1-0272, and by General Motors through the GM/Brown Collaborative Research Laboratory on Computational Materials Research. The authors thank Professor Alan Needleman and Professor Vikram Deshpande for many useful discussions pertaining to this work and for providing the DD code used here.

Appendix: Static Condensation of FE Equations

This appendix describes the implementation of static condensation, which provides for an optimally efficient solution of the EL finite element equations. The incremental FE equations are derived from an expansion of the principle of virtual work, then the elastic degrees-of-freedom (dof) are condensed out, leaving a system of equations for only the cohesive dof. This reduces the size of the system of equations to be solved by two orders of magnitude for the present bimaterial model.

In the superposition method, two finite element solutions are required at each increment for i) the corrective fields of the DD sub-problem and ii) the fields of the EL subproblem. The system of equations for the DD corrective fields is completely linear as the cohesive zone is included only in the EL subproblem. The entire stiffness matrix is constant, can be decomposed once, and stored. The incremental solution for the corrective fields is thus very efficient.

Standard equation solution techniques are, however, largely inefficient for the EL subproblem, which has two linear elastic regions joined by a nonlinear cohesive zone. When only a small subset of the global stiffness matrix is nonlinear (those associated with the cohesive dof), partial decomposition can provide a fast incremental solution. This allows the stiffness decomposition *up to* the first nonlinear dof to be computed once and stored (as it is invariant). In all future increments only the remainder of the stiffness matrix must be decomposed. Clearly for a fixed number of dof, the closer to the end of the matrix the first nonlinear dof appears, the greater the benefit of partial decomposition. In the EL subproblem, optimum node numbering (left to right, top to bottom) places the nonlinear dof in the middle of the unknown nodal dof vector. Even using partial decomposition, over half of the global stiffness matrix must be decomposed during each increment. Due to the large model size (each elastic region has over 20,000 dof) and number of increments required, this is not practical. Instead we use static condensation [31] to obtain a system of equations for only the nonlinear cohesive dof. Once this system is solved, the remaining elastic dof are obtained by matrix multiplication with an appropriate numerical Green's function. This reduces the size of the system of equations to be solved by two orders of magnitude, greatly increasing the efficiency of the EL subproblem incremental solution.

The FE equations are developed from the minimization of potential energy. At time t an elastic body with a cohesive surface S_c, subject to only displacement boundary conditions, has potential energy

$$\Pi^{(t)}=\frac{1}{2}\int_V \sigma_{ij}^{(t)}\epsilon_{ij}\mathrm{d}V-\int_{S_c} T_i^{(t)}u_i\mathrm{d}S_c \tag{A1}$$

The discretizations of the displacement, velocity, and strain fields are

$$u_i=N_{iI}U_I,\quad \dot{u}_i=v_i=N_{iI}\dot{U}_I=N_{iI}V_I,\quad \epsilon_{ij}=u_{i,j}=N_{i,jI}U_I \tag{A2}$$

where U_I and V_I are nodal displacements and velocities, respectively, N_{iI} are the shape functions, and capital indices refer to nodal quantities. Using this discretization in Eq. (A1) gives

$$\Pi^{(t)}=\tfrac{1}{2}K_{IJ}U_IU_J-F_I^cU_I^c \tag{A3}$$

where the global stiffness matrix is $K_{IJ}=\int_V N_{i,jI}C_{ijkl}N_{k,lJ}\mathrm{d}V$, and the global cohesive nodal force vector is $F_I^c=\int_{S_c}T_iN_{iI}\mathrm{d}S_c$.

The incremental equations are obtained by expanding the potential energy at time $t+\Delta t$ about an equilibrium state at time t

$$\begin{aligned}\Pi^{(t+\Delta t)}=\Pi^{(t)}+\Delta t\dot{\Pi}=&\tfrac{1}{2}\int_V\sigma_{ij}\epsilon_{ij}\mathrm{d}V-\int_{S_c}T_iu_i\mathrm{d}S_c\\&+\Delta t\left[\tfrac{1}{2}\int_V\dot{\sigma}_{ij}\epsilon_{ij}\mathrm{d}V+\tfrac{1}{2}\int_V\sigma_{ij}\dot{\epsilon}_{ij}\mathrm{d}V-\int_{S_c}\dot{T}_iu_i\mathrm{d}S_c\right.\\&\left.-\int_{S_c}T_i\dot{u}_i\mathrm{d}S_c\right]\end{aligned} \tag{A4}$$

Rewriting the rate of change of cohesive traction as $\dot{T}_i=\mathrm{d}T_i/\mathrm{d}t=(\mathrm{d}T_i/\mathrm{d}u_j)(\mathrm{d}u_j/\mathrm{d}t)=-k_{ij}^c\dot{u}_j$ allows the cohesive stiffness contribution to be written as $K_{IJ}^{cc}=\int_{S_c}N_{iI}k_{ij}^cN_{iJ}\mathrm{d}S_c$. Using the discretization (A2), Eq. (A4) becomes

$$\Pi^{(t+\Delta t)}=\tfrac{1}{2}K_{IJ}U_IU_J-F_I^cU_I^c+\Delta t[K_{IJ}V_JU_I+K_{IJ}^{cc}V_J^cU_I^c-F_I^cV_I^c] \tag{A5}$$

The standard FE equations could be obtained at this point by minimizing potential energy with respect to nodal displacements, i.e., $d\Pi^{(t+\Delta t)}/dU_K=0$. Here, we use static condensation, which is based on a careful labeling of nodal vectors and matrices according to dof being elastic (i.e., linear, not on the cohesive zone) or cohesive (nonlinear). Then the elastic dof will be condensed out, so that we are left with a system of equations for only the nonlinear cohesive dof.

The total number of dof n is composed of elastic and cohesive dof n_e and n_c, respectively. Any dof can also be classified as belonging to material 1 (upper) or material 2 (lower). Using this notation, the global displacement vector $\mathbf{U}$ can be written as a composition of subvectors

$$\mathbf{U}=\begin{bmatrix}\mathbf{U}^{e(1)}\\ \mathbf{U}^{c(1)}\\ \mathbf{U}^{c(2)}\\ \mathbf{U}^{e(2)}\end{bmatrix},\quad \mathbf{U}^e=\begin{bmatrix}\mathbf{U}^{e(1)}\\ \mathbf{U}^{e(2)}\end{bmatrix},\quad \mathbf{U}^c=\begin{bmatrix}\mathbf{U}^{c(1)}\\ \mathbf{U}^{c(2)}\end{bmatrix} \tag{A6}$$

where $\mathbf{U}$, or any vector, is split into ''local'' vectors $\mathbf{U}^e$ and $\mathbf{U}^c$ formed by the union of subvectors as shown and having respective dimensions of n_e and n_c.

The global stiffness matrix can be similarly decomposed into submatrices as

$$\mathbf{K}=\begin{bmatrix}\mathbf{K}^{ee(1)} & \mathbf{K}^{ec(1)} & \mathbf{0}\\ \mathbf{K}^{ce(1)} & \mathbf{K}^{cc} & \mathbf{K}^{ce(2)}\\ \mathbf{0} & \mathbf{K}^{ce(2)} & \mathbf{K}^{ee(2)}\end{bmatrix} \tag{A7}$$

The relevant local matrices are defined as

$$\mathbf{K}^{ee}=\begin{bmatrix}\mathbf{K}^{ee(1)} & \mathbf{0}\\ \mathbf{0} & \mathbf{K}^{ee(2)}\end{bmatrix},\quad \mathbf{K}^{ec}=\begin{bmatrix}\mathbf{K}^{ec(1)}\\ \mathbf{K}^{ec(2)}\end{bmatrix},$$
$$\mathbf{K}^{ce}=[\mathbf{K}^{ce(1)}\ \ \mathbf{K}^{ce(2)}] \tag{A8}$$

Note that when indicial notation is used to represent a local array, the superscripts denote the range of the indices, e.g., K_{IJ}^{ec} has dimensions $n_e\times n_c$. The cohesive stiffness $\check{K}_{IJ}^{cc}$ necessarily has contributions from the cohesive zone *and* the elastic material. These contributions can be separated as

$$\check{K}_{IJ}^{cc}=K_{IJ}^{cc}+\overline{K}_{IJ}^{cc} \tag{A9}$$

where $\overline{K}_{IJ}^{cc}=\int_V N_{i,jI}C_{ijkl}N_{k,lJ}dV$ is the elastic stiffness contribution to cohesive dof. Local matrices $\mathbf{K}^{ec}$ and $\mathbf{K}^{ce}$ couple elastic and cohesive dof, by construction $\mathbf{K}^{ce}=(\mathbf{K}^{ec})^T$.

The only stiffness submatrix that changes during the incremental procedure is $\check{K}_{IJ}^{cc}$, and all of its variations are contained in K_{IJ}^{cc}. All other stiffness submatrices are strictly a function of elastic constants and undeformed geometry (mesh) and are thus invariant. Rewriting Eq. (*A*5) in local form gives

$$\Pi^{(t+\Delta t)}=\tfrac{1}{2}K_{IJ}^{ee}U_I^eU_J^e+K_{IJ}^{ec}U_J^cU_I^e+\tfrac{1}{2}\overline{K}_{IJ}^{cc}U_I^cU_J^c-F_I^cU_I^c$$
$$+\Delta t[K_{IJ}^{ee}U_I^eV_J^e+K_{IJ}^{ce}V_J^eU_I^c+K_{JI}^{ce}V_J^cU_I^e+\check{K}_{IJ}^{cc}V_J^cU_I^c$$
$$-F_I^cV_I^c] \tag{A10}$$

The FE equations are derived by applying the *two* equilibrium conditions, $d\Pi/dU_K^e=0$ and $d\Pi/dU_K^c=0$, giving

$$K_{IJ}^{ee}V_J^e=-K_{IJ}^{ec}V_J^c-\frac{1}{\Delta t}[K_{IJ}^{ee}U_J^e+K_{IJ}^{ec}U_J^c] \tag{A11}$$

$$\check{K}_{IJ}^{cc}V_J^c=-K_{IJ}^{ce}V_J^e-\frac{1}{\Delta t}[\overline{K}_{IJ}^{cc}U_J^c+K_{IJ}^{ce}U_J^e-F_I^c] \tag{A12}$$

At this point, it is necessary to treat constrained and unconstrained dof separately. Thus all elastic (cohesive) dof $n_e\,(n_c)$ are classified as either constrained $n_{ec}\,(n_{cc})$ or unconstrained $n_{ef}\,(n_{cf})$. For the remainder of this section all implicit summations span only *unconstrained* dof, while summations over constrained dof are written explicitly. The implementation of this convention is best illustrated with a brief example. Consider the sums $K_{IJ}^{ec}V_J^c$ and $\Sigma_{n_{cc}}K_{IJ}^{ec}V_J^c$, which according to our convention span unconstrained and constrained cohesive dof, respectively. The key point is that the matrix K_{IJ}^{ec} (vector V_J^c) has size $n_e\times n_c\,(n_c)$ and contains constrained and unconstrained dof, which are interspersed irregularly. When performing the sum (over unconstrained dof) $K_{IJ}^{ec}V_J^c$, we must inquire at every J as to the existence of a constraint on that particular dof. Only if J is an unconstrained dof is the multiplication performed and the product added to the total for a given I; if J is a constrained dof, then it is skipped over and does not contribute to the sum. It is essential to recall this convention in the following formulation.

The equilibrium Eqs. (*A*11) and (*A*12) are rewritten as

$$K_{IJ}^{ee}V_J^e=-K_{IJ}^{ec}V_J^c-\frac{1}{\Delta t}T_I^e-R_I^e \tag{A13}$$

$$\check{K}_{IJ}^{cc}V_J^c=-K_{JI}^{ec}V_J^e-\frac{1}{\Delta t}T_I^c-R_I^c \tag{A14}$$

where R_I is a nodal force vector and T_I is an equilibrium correction, specifically,

$$R_I^e=\sum_{n_{ec}}K_{IJ}^{ee}V_J^e+\sum_{n_{cc}}K_{IJ}^{ec}V_J^c \tag{A15}$$

$$T_I^e=K_{IJ}^{ee}U_J^e+K_{IJ}^{ec}U_J^c+\sum_{n_{ec}}K_{IJ}^{ee}U_J^e+\sum_{n_{cc}}K_{IJ}^{ec}U_J^c \tag{A16}$$

$$R_I^c=\sum_{n_{ec}}K_{JI}^{ec}V_J^e+\sum_{n_{cc}}\check{K}_{IJ}^{cc}V_J^c, \tag{A17}$$

$$T_I^c=\overline{K}_{IJ}^{cc}U_J^c+K_{JI}^{ec}U_J^e-F_I^c+\sum_{n_{ec}}K_{JI}^{ec}U_J^e+\sum_{n_{cc}}\overline{K}_{IJ}^{cc}U_J^c \tag{A18}$$

Now Eq. (*A*-13) can be solved for V_J^e in terms of V_J^c as

$$V_K^e=-(K_{IK}^{ee})^{-1}K_{IJ}^{ec}V_J^c-\frac{1}{\Delta t}(K_{IK}^{ee})^{-1}T_I^e-(K_{IK}^{ee})^{-1}R_I^e \tag{A19}$$

which is used in Eq. (*A*14) to provide the system of equations for the unconstrained cohesive dof V_J^c

$$[\check{K}_{IJ}^{cc}-K_{KI}^{ec}(K_{LK}^{ee})^{-1}K_{LJ}^{ec}]V_J^c=\frac{1}{\Delta t}[K_{KI}^{ec}(K_{LK}^{ee})^{-1}T_L^e-T_I^c]$$
$$+K_{KI}^{ec}(K_{LK}^{ee})^{-1}R_L^e-R_I^c \tag{A20}$$

where the term in brackets on the left-hand side is an effective stiffness matrix $(n_c\times n_c)$ and the right-hand side is an effective nodal force vector (n_c). Both are known at the beginning of each increment, so the system of Eqs. (*A*20) can be solved for V_J^c. The unknown elastic velocity vector V_J^e is obtained by matrix multiplication from Eq. (*A*13)

$$V_K^e=-(K_{IK}^{ee})^{-1}K_{IJ}^{ec}V_J^c-\frac{1}{\Delta t}(K_{IK}^{ee})^{-1}T_I^e-(K_{IK}^{ee})^{-1}R_I^e \tag{A21}$$

The elastic dof have been condensed out of the system of Eqs. (*A*20) to be solved. Equation (*A*21) involves the numerical Green's function, which, given the cohesive velocity vector V_J^c, outputs the elastic velocity vector V_K^e. An obvious drawback is the fact that the inverse of the elastic stiffness matrix $(K_{LK}^{ee})^{-1}$ must be computed before any incremental solution can begin. This is a huge (symmetric) matrix, but not banded. Before the incremental scheme begins, the elastic stiffness matrix K_{IJ}^{ee} must be inverted, which is significant overhead. Once this has been done,

much of the matrix multiplication, i.e., $K^{ec}_{KI}(K^{ee}_{LK})^{-1}K^{ec}_{LJ}$, $K^{ec}_{KI}(K^{ee}_{LK})^{-1}$, and $(K^{ee}_{IK})^{-1}K^{ec}_{IJ}$ in Eqs. (*A*20) and (*A*21) can be done once and stored. This allows the incremental solution to proceed with optimal efficiency. The static condensation was verified independently of the DD machinery and was in exact agreement with the standard FE method.

References

[1] Stolken, J. S., and Evans, A. G., 1998, ''A Microbend Test Method for Measuring the Plasticity Length Scale,'' Acta Mater., **46**, pp. 5109–5115.

[2] Fleck, N. A., Muller, G. M., Ashby, M. F., and Hutchinson, J. W., 1994, ''Strain Gradient Plasticity: Theory and Experiment,'' Acta Metall. Mater., **42**, pp. 475–487.

[3] Fleck, N. A., and Hutchinson, J. W., 1997, ''Strain Gradient Plasticity,'' J. W. Hutchinson and T. T. Wu, eds., Adv. Appl. Mech., **33**, pp. 295–361.

[4] Gurtin, M. E., 2002, ''A Gradient Theory of Single-Crystal Viscoplasticity That Accounts for Geometrically Necessary Dislocations,'' J. Mech. Phys. Solids, **50**, pp. 5–32.

[5] Acharya, A., and Bassani, J. L., 2000, ''Lattice Incompatibility and a Gradient Theory of Crystal Plasticity,'' J. Mech. Phys. Solids, **48**, pp. 1565–1595.

[6] Shu, J. Y., Fleck, N. A., Van der Giessen, E., and Needleman, A., 2001, ''Boundary Layers in Con-Strained Plastic Flow: Comparison of Nonlocal and Discrete Dislocation Plasticity,'' J. Mech. Phys. Solids, **49**, pp. 1361–1395.

[7] Van der Giessen, E., and Needleman, A., 1995, ''Discrete Dislocation Plasticity: A Simple Planar Model,'' Modell. Simul. Mater. Sci. Eng., **3**, pp. 689–735.

[8] Cleveringa, H. H. M., Van der Giessen, E., and Needleman, A., 1997, ''Comparison of Discrete Dislocation and Continuum Plasticity Predictions for a Composite Material,'' Acta Mater., **45**, pp. 3163–3179.

[9] Cleveringa, H. H. M., Van der Giessen, E., and Needleman, A., 2000, ''A Discrete Dislocation Analysis of Mode I Crack Growth,'' J. Mech. Phys. Solids, **48**, pp. 1133–1157.

[10] Deshpande, V. S., Needleman, A., and Van der Giessen, E., 2002, ''Discrete Dislocation Modeling of Fatigue Crack Propagation,'' Acta Mater., **50**, pp. 831–846.

[11] Benzerga, A. A., Hong, S. S., Kim, K. S., Needleman, A., and Van der Giessen, E., 2001, ''Smaller is Softer: An Inverse Size Effect in a Cast Aluminum Alloy,'' Acta Mater., **49**, pp. 3071–3083.

[12] Bittencourt, E., Needleman, A., Gurtin, M. E., and Van der Giessen, E., 2003, ''A Comparison of Nonlocal Continuum and Discrete Dislocation Plasticity Predictions,'' J. Mech. Phys. Solids, **51**, pp. 281–310.

[13] Eshelby, J. D., 1961, ''Elastic Inclusions and Inhomogeneities,'' *Progress in Solid Mechanics, Vol. II*, I. N. Sneddon and R. Hill, eds., North-Holland, Amsterdam, 89–140.

[14] Shilkrot, L. E., Curtin, W. A., and Miller, R. E., 2002, ''A Coupled Atomistic/Continuum Model of Defects in Solids,'' J. Mech. Phys. Solids, **50**, pp. 2085–2106.

[15] Weygand, D., Friedman, L. H., Van der Giessen, E., and Needleman, A., 2002, ''Aspects of Boundary-Value Problem Solutions With Three-Dimensional Dislocation Dynamics,'' Modell. Simul. Mater. Sci. Eng., **10**, pp. 437–468.

[16] Hirth, J. P., and Lothe, J., 1968, *Theory of Dislocations*, McGraw-Hill, New York.

[17] Rice, J. R., 1988, ''Elastic Fracture Mechanics Concepts for Interfacial Cracks,'' ASME J. Appl. Mech., **55**, pp. 98–103.

[18] Tvergaard, V., and Hutchinson, J. W., 1992, ''The Relation Between Crack Growth Resistance and Fracture Process Parameters in Elastic-Plastic Solids,'' J. Mech. Phys. Solids, **40**, pp. 1377–1397.

[19] Tvergaard, V., and Hutchinson, J. W., 1993, ''The Influence of Plasticity on Mixed Mode Interface Toughness,'' J. Mech. Phys. Solids, **41**, pp. 1119–1135.

[20] Tvergaard, V., and Hutchinson, J. W., 1994, ''Effect of T-Stress on Mode I Crack Growth Resistance in a Ductile Solid,'' Int. J. Solids Struct., **31**, 823–833.

[21] Tvergaard, V., 1997, ''Cleavage Crack Growth Resistance Due to Plastic Flow Around a Near-Tip Dislocation-Free Region,'' J. Mech. Phys. Solids, **45**, pp. 1007–1023.

[22] Tvergaard, V., 1999, ''Effect of Plasticity on Cleavage Crack Growth Resistance at an Interface,'' J. Mech. Phys. Solids, **47**, pp. 1095–1112.

[23] Tvergaard, V., 2001, ''Resistance Curves for Mixed Mode Interface Crack Growth Between Dissimilar Elastic-Plastic Solids,'' J. Mech. Phys. Solids, **49**, pp. 2689–2703.

[24] Suo, Z., Shih, C. F., and Varias, A. G., 1993, ''A Theory for Cleavage Cracking in the Presence of Plastic Flow,'' Acta Metall. Mater., **41**, pp. 1551–1557.

[25] Xu, X.-P., and Needleman, A., 1993, ''Void Nucleation by Inclusion Debonding in a Crystal Matrix,'' Modell. Simul. Mater. Sci. Eng., **1**, pp. 111–132.

[26] Deshpande, V. S., Needleman, A., and Van der Giessen, E., 2001, ''Dislocation Dynamics is Chaotic,'' Scr. Mater., **45**, pp. 1047–1053.

[27] Liechti, K. M., and Chai, Y. S., 1992, ''Asymmetric Shielding in Interfacial Fracture Under In-Plane Shear,'' ASME J. Appl. Mech., **59**, pp. 295–304.

[28] Deshpande, V. S., Needleman, A., and Van der Giessen, E., 2003, ''Discrete Dislocation Plasticity Modeling of Short Cracks in Single Crystals,'' Acta Mater., **51**, 1–15.

[29] Wei, Y., and Hutchinson, J. W., 1997, ''Steady-State Crack Growth and Work of Fracture for Solids Characterized by Strain Gradient Plasticity,'' J. Mech. Phys. Solids, **45**, pp. 1253–1273.

[30] Benzerga, A. A., and Needleman, A., work in progress.

[31] Bathe, K.-J., 1982, *Finite Element Procedures in Engineering Analysis*, Prentice-Hall, Englewood Cliffs, NJ.